Danish Meteorological Institute
Ministry of Transport

Scientific Report 05-07

Operational Processing of CHAMP data: Mathematical Methods, Data Filtering and Quality Control

M. E. Gorbunov

Institute for Atmospheric Physics, Moscow 119017, Russia, gorbunov@dkrz.de

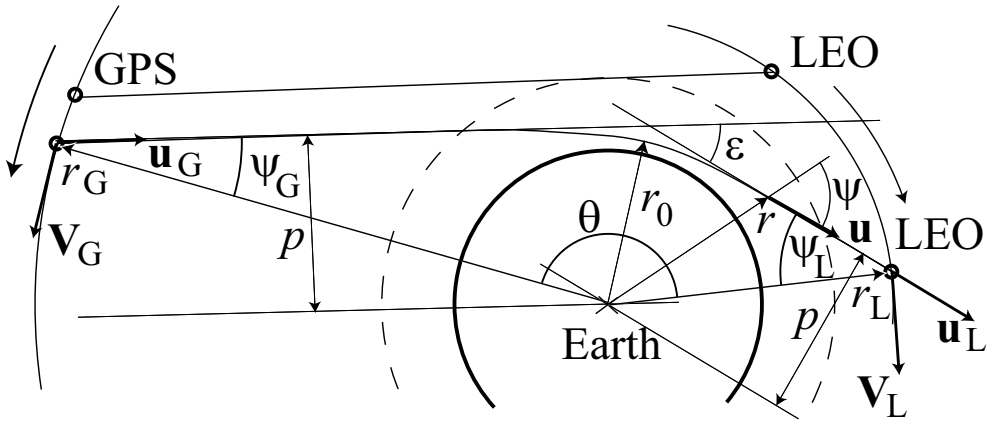

Colophone

Serial title:
Scientific Report 05-07

Title:
Operational Processing of CHAMP data:
Mathematical Methods, Data Filtering and Quality Control

Subtitle:

Authors:
M. E. Gorbunov
Institute for Atmospheric Physics, Moscow 119017, Russia, gorbunov@dkrz.de

Other Contributers:

Responsible Institution:
Danish Meteorological Institute

Language:
English

Keywords:

Url:
www.dmi.dk/dmi/dmi-publikationer.htm

ISSN:
1399-1949

ISBN:
87-7478-526-5

Version:

Website:
www.dmi.dk

Contents

Operational Processing of CHAMP data: Mathematical Methods, Data Filtering and Quality Control

M. E. Gorbunov
Institute for Atmospheric Physics, Moscow 119017, Russia, gorbunov@dkrz.de

1 Introduction

Radio occultations are a very prospective method of the remote sensing of the Earth's atmosphere for Numerical Weather Prediction (NWP) as well as for detection of global climate change [1]. The use of the signals of the Global Positioning System for the remote sensing of the Earth's atmosphere was first suggested in [2]. High stability of the frequency of GPS signals secures the accuracy of the determination of the atmospheric parameters required for the tasks of NWP. The first radio occultation proof-of-concept experiment was conducted in 1995 by UCAR with Microlab-1 satellite [3, 4]. Data acquired by Microlab-1 during 1995–1997 indicated high capabilities of the radio occultation technique [5, 6, 7]. In 2000 Challenging Minisatellite Payload (CHAMP) was launched [8], Currently, CHAMP provides 200–300 occultation events every day.

The underlying physical principle of the radio occultation technique consists in the measurement and interpretation of the amplitude and phase of radio signals transilluminating the Earth's atmosphere. The source of the signals is a GPS satellite, while the receiver is located on a Low-Earth Orbiter (LEO) satellite (the orbit height is about 700 km above the Earth's surface). Wave propagation in the atmosphere is determined by the field of the atmospheric refractivity, which is a known function of the pressure, temperature, and humidity. From measured radio signals, the atmospheric refractivity field can be reconstructed. The humidity term in the refractivity is negligible in polar region at all altitudes, and in tropics above 7–10 km. If humidity is negligible, the hydrostatic equation allows for the retrieval of vertical profiles pressure and temperature from the profile of refractivity. If, however, humidity term is essential, then the use of a priori information (such as background profiles of humidity or temperature from forecast) [4]) or using schemes of variational data assimilation [9, 10, 11, 12]. The basic facts about radio occultation sounding are collected in Chapter 2.1 of this Report.

Interpretation of wave fields measured in radio occultation experiments is performed as follows. First, bending angles are retrieved, and then they are inverted to produce the refractivity profiles. In this Report we describe original algorithms of the determination of bending angles from wave fields, including filtering and quality control.

The simplest approach to the determination of refraction angles is based on the geometric optical (GO) approximation and the assumption of the single ray propagation [13]. This method does not work in the troposphere, where complicated structure of refractivity field results makes the effects of multipath propagation and diffraction essential. The simplest technique of the retrieval of bending angles from wave fields in multipath areas uses the analysis of local spatial spectra in sliding apertures in the framework of the Radio Holographic Synthetic Aperture (RHSA) method [14, 15, 16]. The Canonical Transform (CT) method for the retrieval of the ray structure was introduced in [17]. This method uses the technique of Fourier Integral Operators (FIOs) which allow

for the generalization of the canonical transform formalism used in the geometrical optics, for the wave optics. This method uses a canonical transform that unifies the projection of the ray manifold to the new coordinate axis. The corresponding FIO transform the wave field into the new representation, where there is no multipath propagation. The CT method ensures a high accuracy of the retrieval of bending angles, superior to that provided by the RHSA method.

The CT method was complemented by the Full Spectrum Inversion (FSI) Method introduced in [18]. FSI is based on the fact that in the event of the circular geometry of radio occultation (circular and coplanar orbits of the satellites, and spherical shape of the Earth) the corresponding FIO coincides with the Fourier transform. In order to account for the deviation of the real observation geometry from the circular a further approximation was developed in [18]. A new, 2nd, type of FIOs (FIO2, to be distinguished from the 1st type that had been used before, [17]) was introduced in [19]. FIOs of the 2nd type generalize the FSI method for an arbitrary radio occultation geometry. The accurate solution for the phase function of the FIO2 was found in [20]. The FIO2 with the accurate phase function cannot be reduced to the Fourier transform in the general case. This significantly degrades the numerical efficency of the numerical algorithm.

In Chapter 2.2 we discuss FIOs of the 2nd type. We derive the equations for their phase and amplitude functions and present the solutions. We discuss the connection of FIO2 with canonical transforms. We construct an approximation based on the linearized canonical transform that allows for the reduction of a FIO2 to the Fourier transform, for a generic observation geometry.

Processing real observations requires filtering for noise reduction, as well as identification and sorting out corrupted data. Also, it is necessary to estimation the accuracy of the retrieved bending angles and temperatures. These topics are discussed in Chapter 3.1. This problems are solved by means of the analysis of the local spatial spectra of the measured wave field and the wave field transformed by the FIO2. Although this method does not provide such a high resolution as CT, it is very convenient for visualizing observational data. The spectral width proves to be a very convenient measure of the measurement errors. Therefore, the analysis of the local spatial spectra is complementary to the global methods based on FIOs.

In Chapter 3.2 we give examples of processing CHAMP occultation events. We show how the technique that we describe in this Report is applied for the processing of lower-tropospheric data, where signal tracking errors significantly increase. The plots of spatial spectra visualize the quality of the observational data. We also show retrieved temperatures and their errors.

2 Mathematical Methods of Processing Radio Occultation data

Radio Occultation Basics

During a radio occultation experiment, the satellites moves in such a way that the radio ray linking them immerses into the atmosphere (Fig. 2.1). The phase and the amplitude of the signal are registered and recorded. The experiment is continued until the shadow area is reached, where signal is weak and cannot be reliably measured. The transmitter is located on a GPS satellite, and the space-borne receiver is carried by a Low Earth Orbiter (LEO). The measured wave field is $U(t) = C(t)A(t)\sin(ik\Psi(t) - i\omega t)$, where ω is the transmitter frequency, $A(t)$ is the amplitude of the received signal, $\Psi(t)$ is the optical path along the ray trajectory from the transmitter to the receiver, $C(t)$ is the modulation of the GPS signal by a pseudo-random code. By digital processing, the measured signal $U(t)$ is demodulated and its complex amplitude $u(t) = A(t)\exp(ik\Psi(t))$ is reconstructed [21, 22, 23]. From the full optical path we subtract the vacuum path $\Psi_0(t)$ computed

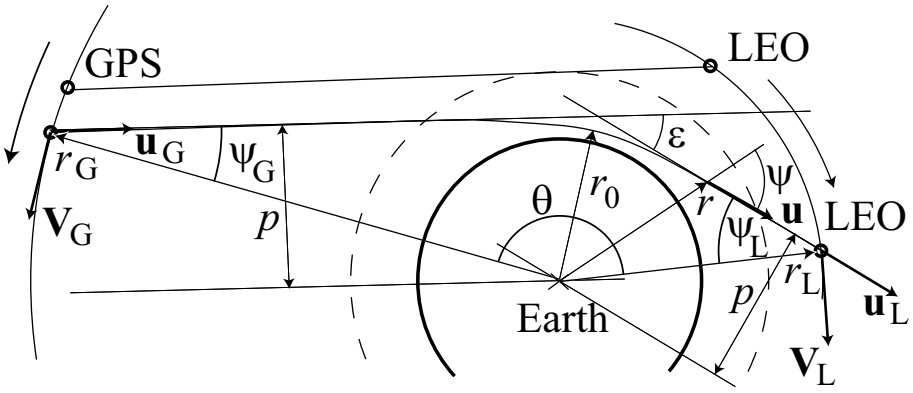

Figure 2.1: Radio occultation geometry

for the straight rays between the transmitter and the receiver. Supplied radio occultation data contain amplitude $A(t)$, atmospheric phase excess $\Delta\Psi(t) = \Psi(t) - \Psi_0(t)$ for the two channels of the GPS (L1 – 1.57542 and L2 – 1.22760 GHz), and the orbit data of the satellites.

In the computation of $\Psi_0(t)$ it is essential to account for the relativistic effects [13]. However, the relativistic factor only depends on the absolute velocity of the satellites. In the difference $\Psi(t) - \Psi_0(t)$ the relativistic effect is cancelled at an relative accuracy of $V^2/c^2 \approx 10^{-9}$. Therefore, if the atmospheric phase excess was correctly computed on the preprocessing stage, we can compute the full optical path $\Psi(t)$ as a sum of $\Delta\Psi(t)$ and the satellite-to-satellite distance, and then use the non-relativistic theory. The relative error of bending angle computation will then be about 10^{-9}, which is 3–4 orders of magnitudes below the main measurement and computational errors.

The derivative of the optical path $\dot{\Psi}$ equals $\mathbf{V}_L\mathbf{u}_L - \mathbf{V}_G\mathbf{u}_G$, where $\mathbf{V}_{L,G}$ are the velocities of the satellite, $\mathbf{u}_{L,G}$ are the unity vectors of ray directions at the transmitter and the receiver (here and after index *G* relates to the GPS satellite, while index *L* relates to the LEO satellite). This expression can be represented as a sum of terms including angular and radial velocity components. From the orbit data of the satellites, we can compute their radial distances from the Earth's center $r_G(t)$ and $r_L(t)$ and the satellite-to-satellite angle $\theta(t) = \theta_L(t) - \theta_G(t)$, where $\theta_G(t)$ and $\theta_L(t)$ are the angular coordinates of the satellites in the instant vertical plane showed in Fig. 2.1. Then we can write the following equation:

$$\dot{\Psi} = \dot{\theta}_L r_L \sin\psi_L - \dot{\theta}_G r_G \sin\psi_G + \dot{r}_L \cos\psi_L + \dot{r}_G \cos\psi_G. \tag{2.1}$$

In the assumption of the local spherical symmetry [24, 25], the impact parameter (leveling height) of the ray p is the same at the transmitter and at the receiver, $p = r_L \sin\psi_L = r_G \sin\psi_G$.. This is a particular case of the formula of Bouger, or Snell's law for a spherically-symmteric medium: $rn(r)\sin\psi = p$, where $n(r)$ is the vertical profile of the atmospheric refractivity. This allows for rewriting the formula for derivative of the optical path as follows:

$$\dot{\Psi} = \eta(p,t) \equiv \dot{\theta}p + \frac{\dot{r}_L}{r_L}\sqrt{r_L^2 - p^2} + \frac{\dot{r}_G}{r_G}\sqrt{r_G^2 - p^2}. \tag{2.2}$$

Here, $\dot{\Psi}$ is the observable quantity, and $\dot{\theta}, \dot{r}_{L,G}, r_{G,L}$ are known functions of time t. Therefore, the right-hand part $\eta(p,t)$ is known function of p and t. Given measurements $\dot{\Psi}(t)$, it is possible to solve equation (2.2) for $p(t)$ (although the solution is non-unique, it is straightforward to choose the only physical solution). The simplest way is to solve equation (2.2) numerically, because its analytical solution is too complicated. The refraction (bending) angle of the ray, ϵ, is defined by the following simple geometrical relation:

$$\epsilon = \theta - \arccos\frac{p}{r_L} - \arccos\frac{p}{r_G}. \tag{2.3}$$

From the known function $p(t)$ and orbit data $r_G(t), r_L(t), \theta(t)$ we can thus determine the bending angles $\epsilon(t)$. Functions $p(t)$ and $\epsilon(t)$ specify the profile of bending angle $\epsilon(p)$, parametrically. The above discourse was essential based on the assumption that at each moment of time t only one ray is observed. In the event of interference of multiple rays, the computation of bending angles from the derivative of the optical path results in non-physical, strongly oscillating profiles [17]. The methods of the determination of bending angle profiles in multipath areas are discussed below in Chapter 2.2.

By the Abel transform, from the bending angle profile it is possible to derive the profile of the refractivity [26]:

$$n(x) = \frac{1}{\pi} \exp\left(\int_x^\infty \frac{\epsilon(p)\, dp}{\sqrt{p^2 - x^2}} \right), \tag{2.4}$$

where $x(r) = rn(r)$ is the refractive radius. The retrieved profile $n(x)$ and the dependency $r(x) = x/n(x)$ define the profile $n(r)$ in the parametric form.

In this Report, we do not discuss the retrieval of the atmospheric humidity. If the influence of humidity is negligible, then the refractive index is computed as follows [27]:

$$n = 1 + C\frac{P}{T} = 1 + CR\rho, \tag{2.5}$$

where P is the pressure, T is the temperature, R is the gas constant for the dry air, ρ is the density, $C = 77.6 \times 10^{-6}$ hPa/K. From here, together with the hydrostatic and state equations, we obtain the temperature [24]:

$$T(z) = \frac{\int_z^\infty g(z')\rho(z')\, dz'}{R\rho(z)} = \frac{\int_z^\infty g(z')\,[n(z') - 1]\; dz'}{R\,[n(z) - 1]}, \tag{2.6}$$

where $z = r - r_E$ is the altitude above the Earth's surface, $g(z)$ is the profile of the gravity acceleration.

Reconstruction of Ray Structure of Wave Fields

Multipath Propagation

In presence of complicated profiles of refractivity $n(r)$, the corresponding bending angle profiles $\epsilon(p)$ is a non-monotonous function. This results in multipath propagation of radio signals [14]. In order to show this, consider the geometric relation (2.3). Given profile $\epsilon = \epsilon(p)$ and some positions of the transmitter and receiver defined by the parameters r_L, r_G, θ, (2.3) will be an equation for the the impact parameters of all the rays linking the transmitter and the receiver. Denote the right-hand part of (2.3) $\epsilon_G(p)$. Define $D_{G,L} = \sqrt{r_{G,L}^2 - p^2}$ the distances from the transmitter and the receiver to the planet limb and $D = \left(D_L^{-1} + D_G^{-1}\right)^{-1}$ the reduced observation distance. Then we can write the following equation:

$$\frac{d\epsilon_G(p)}{dp} = \frac{1}{D} > 0. \tag{2.7}$$

This shows that $\epsilon_G(p)$ is a monotonously increasing function of the impact parameter. For a smooth exponential model of the atmosphere, $\epsilon(p)$ monotonously decreases, $d\epsilon(p)/dp < 0$. Therefore, dependencies $\epsilon(p)$ and $\epsilon_G(p)$ for each satellite configuration have not more than one intersection point. In this case there is a single-ray propagation. If, however, dependence $\epsilon(p)$ is non-monotonous and there exist such p that $d\epsilon(p)/dp > D^{-1}$, then observation points exist, where multiple rays are observed. From this it follows that if the observation distance is large enough, then a non-monotonous profile $\epsilon(p)$ should necessarily result in multipath propagation.

Analysis of Local Spatial Spectra of Wave Field

The wave field in a multipath area can be approximately written as a sum of fields corresponding to different interfering rays:

$$u(t) = \sum_j u_j(t) = \sum_j A_j(t) \exp\left(ik\Psi_j(t)\right), \tag{2.8}$$

where index j enumerates the rays with impact parameters $p_j(t)$ observed at time moment t. For functions $p_j(t)$ and $\dot{\Psi}_j(t)$, relation (2.2) holds. However, the the expansion of the full measured field $u(t)$ into components $u_j(t)$, as well as the number of the components are unknown a priori. Therefore, equation (2.2) cannot be directly used for the determination of the impact parameters. It is also straighforward that in a multipath area we cannot substitute the derivative of the eikonal $\dot{\Psi}(t)$ of the field $u(t)$ into equation (2.2), which is only valid for single-ray propagation.

The simples way of the separation of interfering rays implements the analysis of local spatial spectra of the wave field. This method was used for processing data of sounding of planetary atmospheres [28]. For the application for sounding the Earth's atmosphere, this method was enhanced by using the focused synthetic aperture [14, 15, 29, 30]. In the framework of this technique, a spectral analysis of the wave field $u(t)$ in sliding apertures is performed:

$$v(t,\eta) = \int_{t-T/2}^{t+T/2} \frac{u(\tau)\cos\dfrac{\pi\left(\tau - t\right)}{T}}{A_m(\tau)\exp\left[ik\left(\Psi_m(\tau) - \dot{\Psi}_m(t)\tau\right)\right]} \exp\left(-ik\eta\tau\right) d\tau, \tag{2.9}$$

where $A_m(t)\exp\left(ik\Psi_m(t)\right)$ is the reference signal, computed for a smooth model of atmospheric refractivity, T is the sliding aperture size. The use of the reference signal is essential, because it corrects for the wave front curvature and thus it focuses the synthesized aperture [15, 29]. The maxima of the spectrum $|v(t,\eta)|$ for each time t expose the physical rays interfering in given observation point. The impact parameter p and bending angle ϵ can be expressed as functions $p(t,\eta)$ and $\epsilon(t,\eta)$ from equations (2.2, 2.3). This is a parametric form of the amplitude of the local spatial spectrum as function $|v(p,\epsilon)|$. This method imposes some restrictions on the resolution [29], however, it is an extremely convenient means of the visualization and diagnostics of experimental data [31].

Canonical Transform Method

For the reconstruction of the ray structure of wave fields we use the Canonical Transform (CT) method [17, 19]. The general description of the method follows. We measure the wave field $u(y) = A(y)\exp(ik\Psi(y))$ along the satellite parameterized by some arbitrary coordinate y (in particular, we can choose $y = t$). It is necessary to determine its ray structure, i.e. the ray directions at each point y. In the framework of the Hamilton formulation of the geometric optics, ray are described by the canonical Hamilton system with respect to coordinate y and momentum η [32]. Momentum equals the derivative of the eikonal $\partial\Psi/\partial y$ provided that at point y only one ray is observed [32]. In event of interference of multiple rays, their momenta η_j are according to equation (2.8) as $\partial\Psi_j/\partial y$. Multiple rays emerge if the projection of the ray manifold to axis y is multi-valued [33]. Formula $\eta = \partial\Psi/\partial y$ is inapplicable in this case. A canonical transform of the coordinate and momentum in the phase space allows for choosing new coordinate z and momentum ξ in such a way that the projection of the ray manifold to the new coordinate axis is single-valued [17]. The corresponding transform of the wave field is performed by the FIO $\hat{\Phi}$. From the transformed wave field $\hat{\Phi}u(z) = A'(z)\exp\left(ik\Psi'(z)\right)$ it is possible to compute the momentum in the new representation $\xi(z) = \partial\Psi'/\partial z$. This allows for the reconstruction of the complete ray manifold. Using the inverse

canonical transform, it can be mapped back into the representation of the old coordinate and momentum.

In work [17] an FIO was used, which it was afterwards suggested to term FIO of the 1st type [19]. The operator was employed in combination with the back propagation. As a generalization of the FSI method [18], in [19] FIOs of the 2nd type were introduced. These operators are applied directly to measured wave field $u(t)$ without back propagation, which allow for the enhancement of the numerical efficiency.

FIO of the 2nd type has the following form:

$$\hat{\Phi}_2 u(z) = \sqrt{\frac{-ik}{2\pi}} \int a_2(z,t) \exp(ikS_2(z,t)) u(t)\, dt, \tag{2.10}$$

where $a_2(z,t)$ is the amplitude function, and $S_2(z,t)$ is the phase function of the operator. Consider the link between this operator and canonical transforms. For this purpose we employ the stationary phase method. For the sake of simplification of the notation, we consider the field $u(t)$, assuming that, if necessary, we can consider its component $u_j(t)$. The stationary phase point $t_s(z)$ of the integral (2.10) is defined by the following equation:

$$\frac{\partial S_2(z,t)}{\partial t} = -\frac{d\Psi(t)}{dt} \equiv -\eta(t). \tag{2.11}$$

Let $\hat{\Phi}_2 u(z) = A'(z) \exp\left(ik\Psi'(z)\right)$. The eikonal Ψ' of the transformed wave field $\hat{\Phi}_2 u(z)$ is computed as follows:

$$\Psi'(z) = S_2(z, t_s(z)) + \Psi(t_s(z)) + \frac{\gamma}{k}, \tag{2.12}$$

where $\gamma = \pm\pi/2$. Term γ/k asymptotically vanishes with big wavenumbers k, and for our analysis it is not essential. Compute the derivative of the eikonal, i.e. the momentum $\xi(z)$ of the transformed wave field, using equation (2.11):

$$\xi(z) \equiv \frac{d\Psi'(z)}{dz} = \frac{dt_s}{dz}\left(\frac{\partial S_2(z,t)}{\partial t} + \frac{d\Psi(t)}{dt}\right)\Big|_{t=t_s(z)} + \frac{\partial S_2(z,t)}{\partial z}\Big|_{t=t_s(z)} = \frac{\partial S_2(z,t_s(z))}{\partial z}. \tag{2.13}$$

From (2.11) and (2.13) we derive we derive the following equation for the full differential of the phase function:

$$dS_2 = \xi\, dz - \eta\, dt. \tag{2.14}$$

Here, $\eta\, dt$ is the reduced form of action in the old representation. Similarly, $\xi\, dz$ is the reduced form of action in the representation of the transformed coordinate z. Because the difference $\xi\, dz - \eta\, dt$ equals a full differential dS_2, the transform $(t,\eta) \to (z,\xi)$ is canonical [34]. A detailed analysis of the link between FIOs and canonical transforms can be found in [35].

Amplitude function is determined from the energy conservation principle:

$$\left|\hat{\Phi}_2 u(z)\right|^2 dz = |u(t_s(z))|^2\, \mu\, dt_s(z), \tag{2.15}$$

where $\mu = \mu(z,t)$ is the measure density, which will be defined below. Using the standard expression for the amplitude in the approximation of the stationary phase, we derive the following equation:

$$\left.\frac{|a_2(z,t)A(t)|^2}{\left|-\dfrac{\partial^2 S_1(z,t)}{\partial t^2} - \dfrac{d^2\Psi(t)}{dt^2}\right|}\right|_{t=t_s(z)} dz = A^2(t_s(z))\, |\mu\, dt_s(z)|\,. \tag{2.16}$$

Therefore, we arrive at the following formula for the amplitude function:

$$|a_2(z,t_s(z))|^2 = \left| -\frac{\partial^2 S_1(z,t)}{\partial t^2} - \frac{d^2\Psi(t)}{dt^2}\bigg|_{t=t_s(z)} \right| \left| \frac{\mu\, dt_s(z)}{dz} \right|. \tag{2.17}$$

Differentiating equation for the stationary phase point (2.11) with respect to z, we derive the following equation:

$$\left(\frac{\partial^2 S_1(z,t)}{\partial t^2} + \frac{d^2\Psi(t)}{dt^2} \right)\bigg|_{t=t_s(z)} \frac{dt_s(z)}{dz} = -\frac{\partial^2 S_1(z,t)}{\partial z\, \partial t}\bigg|_{t=t_s(z)}. \tag{2.18}$$

Using it, we can write the ultimate formula for the amplitude function:

$$a_2(z,t) = \sqrt{\left| \mu \frac{\partial^2 S_2(z,t)}{\partial z\, \partial t} \right|}. \tag{2.19}$$

Now we apply the technique of FIOs for the reconstruction of the ray structure of the measured wave field $u(t)$. At every moment of time t several rays with different impact parameters p can interfere. Impact parameters of different rays in a spherically-symmetric medium are always different. This follows from the fact that impact parameters of rays leaving the transmitter equal $p = r_G \sin\psi_G$. Because different rays have different start direction ψ_G, they will also have different impact parameters. Because the impact parameter of a ray is the same at the transmitter and at the receiver, all the rays registered during a radio occultation experiment have different impact parameters.

Consider a ray manifold in the phase space with coordinate t and momentum η. Multipath propagation takes place if the projection of the ray manifold to the axis t is multi-valued. If we consider the new coordinate $z = p$, then, as was shown above, the projection of the ray manifold to axis p is single-valued. Therefore, we will use the canonical transform $(t,\eta) \to (p,\xi)$, where the new momentum ξ will be determined below from the requirement for the transform to be canonical.

Because the FIO must conserve energy, we begin with the definition of the measure density μ. Denote the power of the transmitter P. We require energy conservation in the following form:

$$\frac{P}{2\pi} dp = A^2 \mu\, dt. \tag{2.20}$$

Energy transmitted by an omnidirectional antenna in an infinitesimal cone is given by the following expression [36]:

$$dE_T = \frac{P}{4\pi} d\psi_G \sin\psi_G\, d\phi, \tag{2.21}$$

Impact parameter p equals $r_G \sin\psi_G$. From this, we derive $dp = r_G \cos\psi_G d\psi_G = \sqrt{r_G^2 - p^2}\, d\psi_G$. Therefore, we have the following distribution of the energy with respect to impact parameters:

$$dE_T = \frac{P}{4\pi} \frac{1}{\sqrt{r_G^2 - p^2}} \frac{p}{r_G}\, d\phi\, dp. \tag{2.22}$$

Consider a receiving aperture in the form of an infinitesimal element of a sphere concentric with the Earth. (Fig. 2.2). The received energy equals $A^2 \cos\psi_L\, dS$, where A is the refractive amplitude, ψ_L

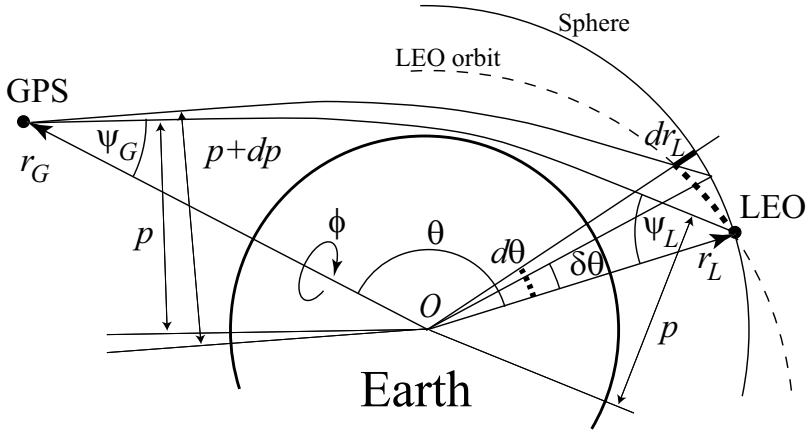

Figure 2.2: Ray tube geometry for the definition of the amplitude of radio occultation signal.

is the angle between the ray tube and the normal to the receiving aperture, dS is the square of the receiving aperture [36]:

$$dE_R = \frac{1}{2}A^2 \cos\psi_L r_L r_L \sin\theta\, d\phi\, \delta\theta = \frac{1}{2}A^2\sqrt{r_L^2 - p_L^2}\, r_L \sin\theta\, d\phi\, \delta\theta. \tag{2.23}$$

Here δ denotes the differential along the sphere with constant r_L, r_G. Employing the identity between the transmitted and received energy, we derive the following expression for the amplitude:

$$A^2 = \frac{P}{2\pi}\frac{1}{\sqrt{r_L^2 - p^2}\sqrt{r_G^2 - p^2}}\frac{p}{r_G r_L \sin\theta}\frac{dp}{\delta\theta} \equiv \frac{P}{2\pi}\frac{dp}{\mu\, dt}. \tag{2.24}$$

For the size of the the virtual receiving aperture $\delta\theta$ we have the following expression:

$$\delta\theta = d\theta - \left(\frac{\partial\theta}{\partial r_G}\right)_p dr_G - \left(\frac{\partial\theta}{\partial r_L}\right)_p dr_L = d\theta - \frac{dr_G}{r_G}\frac{p}{\sqrt{r_G^2 - p^2}} - \frac{dr_L}{r_L}\frac{p}{\sqrt{r_L^2 - p^2}}. \tag{2.25}$$

From this, we derive the following expression for the measure density:

$$\mu = \sqrt{r_L^2 - p^2}\sqrt{r_G^2 - p^2}\frac{r_L r_G}{p}\sin\theta\left(\dot\theta - \frac{\dot r_G}{r_G}\frac{p}{\sqrt{r_G^2 - p^2}} - \frac{\dot r_L}{r_L}\frac{p}{\sqrt{r_L^2 - p^2}}\right). \tag{2.26}$$

Using equations (2.14, 2.2), we derive the phase function [20, 35]:

$$\begin{aligned} S_2(p,t) = -\int \eta(p,t)\, dt = -\int\left(p d\theta + \frac{dr_G}{r_G}\sqrt{r_G^2 - p^2} + \frac{dr_L}{r_L}\sqrt{r_L^2 - p^2}\right) = \\ = -p\theta - \sqrt{r_G^2 - p^2} + p\arccos\frac{p}{r_G} - \sqrt{r_L^2 - p^2} + p\arccos\frac{p}{r_L}. \end{aligned} \tag{2.27}$$

This expression is defined up to an arbitrary function $F(p)$, which it is convent to assume being identically equal to 0. Denote $t_s(p)$ the trajectory point where the ray with a prescribed impact parameter p is observed. The derivative of the eikonal of the transformed wave field $\hat\Phi_2 u(p)$, or the new momentum ξ, due to formulas (2.14), is computed as follows [20, 35]:

$$\xi(p) = \left.\frac{\partial S_2(p,t)}{\partial p}\right|_{t=t_s(p)} = -\theta + \arccos\frac{p}{r_G} + \arccos\frac{p}{r_L} = -\epsilon(p). \tag{2.28}$$

Therefore, for the processing of radio occultation data, it is possible to apply the operator of the 2nd type and compute the transformed wave field $\hat{\Phi}_2 u(p) = A'(p)\exp(ik\Psi'(p))$. The derivative of its eikonal $\Psi'(p)$ with the negative sign is equal to the refraction angle $\epsilon(p)$. The phase function is defined up to an an arbitrary function $F(p)$. Therefore, the phase function can be redefined $S_2'(p,t) = S_2(p,t) + F(p)$. In this case momentum equals $\xi' = \xi + dF(p)/dp$. This correspond to the multiplication of $\hat{\Phi}_2 u(p)$ with $\exp(ikF(p))$. The bending angle is then equal to $\epsilon(p) = -\xi' + dF(p)/dp$. Thus, the new momentum is defined up to an arbitrary function of the impact parameter.

By virtue of the definition of the amplitude function $a_2(p,t)$ by formulas (2.15, 2.20), the amplitude of the transformed field $\left|\hat{\Phi}_2 u(p)\right|$ is close to the θ-function. In the light zone it is approximately constant, in the shadow zone it abruptly drops to very small values [31].

For a circular observation geometry ($r_G = \text{const}$, $r_L = \text{const}$) the phase function linearly depends on θ, and in the amplitude the dependence from θ is factored out:

$$\hat{\Phi}_2 u(p) = \sqrt{\frac{-ik}{2\pi}}\exp\left[ik\left(-\sqrt{r_G^2-p^2}+p\arccos\frac{p}{r_G}-\sqrt{r_L^2-p^2}+p\arccos\frac{p}{r_L}\right)\right]\times$$
$$\times\left(\sqrt{r_L^2-p^2}\sqrt{r_G^2-p^2}\frac{r_L r_G}{p}\right)^{1/2}\int\exp(-ikp\theta(t))u(t)\sqrt{\sin(\theta(t))}\dot{\theta}(t)\,dt. \quad (2.29)$$

This reduces the operator to the combination of the Fourier transform of $u(t(\theta))\sqrt{\sin\theta}$ with respect to the variable θ and multiplication with a known function of p. We will describe an approximation that allows for the reduction of the FIO to the Fourier transform for an arbitrary observation geometry.

From equation (2.2) the impact parameter p can be expressed as function $p(t,\eta)$. Introduce the approximate value of the impact parameter $\tilde{p}$:

$$\tilde{p}(t,\eta) = p_0(t) + \frac{\partial p_0}{\partial\eta}(\eta-\eta_0(t)) = f(t) + \frac{\partial p_0}{\partial\eta}\eta,$$

$$f(t) = p_0(t) - \left.\frac{\partial p_0}{\partial\eta}\right|_{\eta=\eta_0(t)}\eta_0(t) = p_0 - \left(\dot{\theta} - \frac{\dot{r}_G}{r_G}\frac{p_0}{\sqrt{r_G^2-p_0^2}} - \frac{\dot{r}_L}{r_L}\frac{p_0}{\sqrt{r_L^2-p_0^2}}\right)^{-1}\eta_0. \quad (2.30)$$

where $\eta_0(t)$ is a smooth model of the derivative of the optical path, $p_0(t) = p(t,\eta_0(t))$. Model $\eta_0(t)$ can be obtained by the differentiation of the measured optical path with a strong smoothing. The accuracy of this approximation for the impact parameter is about 1 m for a typical observation geometry. Define a new parameter of the trajectory $Y = Y(t)$ and the corresponding momentum σ as follows:

$$dY = \left(\frac{\partial p_0}{\partial\eta}\right)^{-1}dt = \frac{\partial\eta}{\partial p_0}dt, \quad (2.31)$$

$$\sigma = \frac{\partial p_0}{\partial\eta}\eta. \quad (2.32)$$

For the sake of simplicity, we use notation $u(Y)$ instead of $u(t(Y))$. For the transform into the representation of the approximate impact parameter, we introduce a linear canonical transform:

$$\tilde{p} = f(Y) + \sigma, \quad (2.33)$$

$$\xi = -Y, \quad (2.34)$$

Its generating function is defined by equation (2.14):

$$dS_2 = \xi\, d\tilde{p} - \eta\, dY = -Y\, d\tilde{p} - (\tilde{p} - f(Y))\, dY, \tag{2.35}$$

$$S_2(\tilde{p}, Y) = -\tilde{p}Y + \int_0^Y f(Y')\, dY'. \tag{2.36}$$

For dY we have the following expression:

$$dY = d\theta - \frac{dr_G}{r_G}\frac{p_0}{\sqrt{r_G^2 - p_0^2}} - \frac{dr_L}{r_L}\frac{p_0}{\sqrt{r_L^2 - p_0^2}} \approx \delta\theta. \tag{2.37}$$

We can write approximately $\delta\theta/dY \approx 1$. Because $|\partial^2 S_2/\partial\tilde{p}\,\partial Y| = 1$, the amplitude function equals $\sqrt{\mu}$:

$$a_2(\tilde{p}, Y) = \left(\sqrt{r_L^2 - \tilde{p}^2}\sqrt{r_G^2 - \tilde{p}^2}\frac{r_L r_G \sin\theta}{\tilde{p}}\right)^{1/2}. \tag{2.38}$$

The amplitude function $a_2(\tilde{p}, Y)$ in operator $\hat{\Phi}_2$ can be replaced with $a_2(\tilde{p}, Y_s(\tilde{p}))$ and factored out from within the integral. The resulting operator will be a composition of the multiplication with a reference signal $\exp\left[ik\int f(Y)\, dY\right]$, the Fourier transform and multiplication with the amplitude function:

$$\hat{\Phi}_2 u(\tilde{p}) = \sqrt{\frac{-ik}{2\pi}} a_2(\tilde{p}, Y_s(\tilde{p})) \int \exp(-ik\tilde{p}Y) \exp\left(ik\int_0^Y f(Y')\, dY'\right) u(Y)\, dY. \tag{2.39}$$

Function $Y_s(\tilde{p})$ equals $-\xi$, where momentum ξ is equal to the derivative of the eikonal of the transformed wave field. For the computation of the eikonal, we first substitute 1 instead of $a_2(\tilde{p}, Y_s(\tilde{p}))$ into (2.39), then compute momentum ξ and multiply the transformed wave function with $a_2(\tilde{p}, Y_s(\tilde{p}))$. The bending angle ϵ as a function of p and Y is defined by relation (2.3) and orbit data $r_G(t(Y))$, $r_L(t(Y))$ and $\theta(t(Y))$. Substituting $Y = Y_s(p)$, we arrive at the profile of the bending angle $\epsilon(p)$:

$$\epsilon(p) = \theta\left(t(Y_s(p))\right) - \arccos\frac{p}{r_L\left(t(Y_s(p))\right)} - \arccos\frac{p}{r_G\left(t(Y_s(p))\right)} \tag{2.40}$$

3 Analysis of CHAMP data

Filtering and Quality Control of CHAMP Data

Introduction

In this Chapter we demonstrate how the technique that we have developed above is employed for the analysis of the observational data acquired by CHAMP. The measurement of radio occultation signals in multipath areas, where the amplitude and phase of the signal undergo strong fluctuations, poses a technical challenge. Under these conditions, the receiver often loses the track of the signal or corrupts the data [21, 22]. The quality of CHAMP data in the troposphere below 10 km proves to be degraded [37, 23, 38]. L2 channel is especially susceptible to signal tracing errors. Therefore, data processing chain must contain filtering and quality control components.

Observational data contain orbit data of the satellites, amplitudes $A_{1,2}(t_i)$, atmospheric phase excesses $\Delta\Psi_{1,2}(t_i)$ for L1 and L2 channels at a sampling rate of 50 Hz ($t_i = t_0 + 0.02i$ seconds.). Full optical paths are computed as $\Psi_{1,2}(t_i) = \Psi_0(t_i) + \Delta\Psi_{1,2}(t_i)$, where $\Psi_0(t_i)$ is the transmitter-to-receiver distance. The velocity of the vertical immersion of the ray into the atmosphere is estimated as 2 km/s under the conditions of weak refraction above 10 km. This corresponds to a spatial sampling rate of about 40 m. In the troposphere, due to strong regular refraction, the velocity of the ray immersion decreases down to 0.2 km/s on the average, near the Earth's surface.

The data processing chain contains the following blocks: 1) Preprocessing. The final fragments of occultation data sets measured in the lower troposphere, where signal tracking errors are essential are cut-off. A correction is applied to the data measured in the L2 channel, where signal tracking errors significantly exceed those in the L1 channel. 2) Retrieval of bending angles with the aid of the FIO technique described in Chapter 2.2. 3) Estimation of bending angles by the analysis of the local spatial spectra of the transformed wave fields $\hat{\Phi}_2 u_1(p)$. 4) The inversion of bending angles and the estimation of the errors of the retrieved temperature from the bending angle errors.

Preprocessing of Observational Data

A rough estimation of the refraction angle profile is performed by equations (2.2) and (2.3), where $\dot{\Psi}$ is evaluated with a strong smoothing with a vertical filter width of about 2 km. Starting from the moment of time, where the bending angle estimate reaches 0.02 rad, data are cut-off. Statistical analysis [38] indicates that such data are unsuitable for further processing.

Then the analysis of the local spatial spectra $v_{1,2}(t, \eta)$ is performed for the signals $u_{1,2}(t) = A_{1,2}(t) \exp[ik_{1,2}\Psi_{1,2}(t)]$. An example of the spectra is shown in Fig. 3.1 in panels a) and b). The spectra are plotted in pseudo-color (gray scale) in coordinates ϵ, p by using the dependencies $\epsilon(t, \eta)$ and $p(t, \eta)$. Instead of the impact parameter p we use the ray (leveling) height $p - r_E$, where r_E is the radius of local curvature of the geoid. The ray that touches the Earth's surface with its perigee point has an ray height of $r_E(n(r_E) - 1) \simeq 2$ km, because the characteristic value of the refractive index n on the Earth's approximately equals $1 + 3 \times 10^{-4}$, and $r_E \simeq 6370$ km. In the L1 channel, the spectra especially well visualize the refraction angle profile above 6.5 km. In the L2 channel this fragment of the bending angle profile is also distinctly seen. However, the spectra are wider as compared to L1, which indicates a worse signal quality. Below 6.5 km the L1 spectra reveal a complicated structure, which an evidence of multipath propagation. In the L2 channel the situation is completely different. After the ray height reaches 6.5 km and the refraction angle 0.011 rad, the

spectra indicate a rapid increase of the refraction angle, also resulting in overestimated ray heights, because for a fixed observation point rays with a greater bending angle come form a greater height. This signifies that the L2 signal was lost, and this fragment of the L2 signal record is unsuitable for processing. For sorting out such data, we form a penalty function characterizing the L2 data quality. From the spectra we evaluate the mean value and the spectral width of the impact parameter:

$$\bar{p}_{1,2}(t) = \frac{\int |v_{1,2}(t,\eta)|^2 \, p(t,\eta)\, d\eta}{\int |v_{1,2}(t,\eta)|^2 \, d\eta}, \tag{3.1}$$

$$\delta p_{1,2}(t) = \left(\frac{\int |v_{1,2}(t,\eta)|^2 \, (p(t,\eta) - \bar{p}_{1,2}(t))^2 \, d\eta}{\int |v_{1,2}(t,\eta)|^2 \, d\eta} \right)^{1/2}. \tag{3.2}$$

The empirical penalty function is assumed to be equal to the following expression:

$$W(t) = 1 - \exp\left[-\frac{(\bar{p}_2(t) - \bar{p}_1(t))^2 + \delta p_2^2(t)}{\Delta p^2} \right], \tag{3.3}$$

where parameter Δp equals 0.2 km. This function estimation the degradation of the quality in the L2 channel. The indicators of the quality degradation are a large spectral width $\delta p_2(t)$ and a large discrepancy between L1 and L2 impact parameters $\bar{p}_2(t) - \bar{p}_1(t)$.

The smoothed optical paths are computed from the profiles of the smoothed impact parameter:

$$\bar{\Psi}_{1,2}(t) = \int_{t_0}^{t} \eta(\bar{p}_{1,2}(t'), t')\, dt'. \tag{3.4}$$

Smoothed ionospheric difference of the optical paths is evaluated as $\Delta\bar{\Psi}(t) = \bar{\Psi}_2(t) - \bar{\Psi}_1(t)$ in the time interval where $W(t) < 0.7$. In the troposphere, where the L2 signal quality is typically degraded ($W(t) > 0.7$), $\Delta\bar{\Psi}(t)$ is linearly extrapolated. For this purpose, a linear regression $\Delta\bar{\Psi}(t)$ is constructed between the moment of time, when the ray reaches a height of 30 km, and the moment of time, when $W(t)$ reaches a value of 0.7.

Denote D_i the operation of taking the finite difference of a gridded function $D_i F = F(t_{i+1}) - F(t_i)$. The corrected optical path $\Psi_2^{cor}(t)$ and amplitude $A_2^{cor}(t)$ for the L2 channel are defined as a linear combination of L1 and L2 data with a weight determined by the penalty function $W(t)$:

$$D_i\Psi_2^{cor} = D_i\Psi_2\,(1 - W(t_i)) + \left(D_i\Psi_1 + D_i\Delta\bar{\Psi}\right) W(t_i), \tag{3.5}$$

$$\Psi_2^{cor}(t_i) = \sum_{j=1}^{i-1} D_j\Psi_2^{cor}, \tag{3.6}$$

$$A_2^{cor}(t_i) = A_2(t_i)\,(1 - W(t_i))\,. \tag{3.7}$$

The definition of the combination in terms of the finite differences allows for getting rid of the arbitrary constants $\Psi_{1,2}^0$ in the L1 and L2 optical paths. The linear combination of the optical paths will contain the combination of the constants $\Psi_2^0\,(1 - W(t_i)) + \Psi_1^0 W(t_i)$, which is not constant, which results in significant errors in the computation of the refraction angle.

Determination of Bending Angles

Wave fields $u_1(t)$ and $u_2^{cor}(t)$ are transformed by the FIO $\hat{\Phi}_2$, defined by formulas (2.39), (2.38) and (2.30). The bending angles $\epsilon_{1,2}(p)$ are computed by formula (2.40). The border of the geometric

optical shadow p_1 is defined as the maximum of the correlation of the amplitude $\left|\hat{\Phi}_2 u_1(p)\right|$ with the θ-function. For the L2 data, the correlation maximum of $\left|\hat{\Phi}_2 u_1(p)\right|$ with the θ-function, p_2, defines the border, below which the L2 data are unsuitable for further processing (typically, $p_2 > p_1$). For $p \in [p_1, p_2]$ the L2 bending angles $\epsilon_2(p)$ were defined as $\epsilon_1(p) + \Delta\epsilon(p)$, where $\Delta\epsilon(p)$ is the estimation of the ionospheric difference $\epsilon_1(p) - \epsilon_2(p)$ computed by average over the interval of impact parameters $[p_1, p_1 + 1 \text{ km}]$.

Bending angle profiles $\epsilon_{1,2}(p)$ contain the ionospheric component, which is inversely proportional to the squared frequency, if we assume that bending angle is approximately a linear functional of the ionospheric refractivity. This allows for the extraction of the neutral component of the bending angle $\epsilon(p)$ [39, 40, 41, 42]. Above 50 km the ionospheric component of refraction angle significantly exceeds the neutral component. This allows for the estimation of the residual ionospheric error $\delta\epsilon_I(p)$ in the bending angle profile $\epsilon(p)$ [41].

Estimation of Bending Angle Errors

The estimation of errors of $\epsilon(p)$ in the lower troposphere is performed by the analysis of local sliding spectra of the transformed wave field $\hat{\Phi}_2 u_1(p) = A'(p) \exp(ik\Psi'(p))$. For this purpose we computed eikonal $\bar{\Psi}'(p)$ smoothed with a window of 0.25 km and the sliding spectra similar to (2.9):

$$w(p,\xi) = \int_{p-\Delta p/2}^{p+\Delta p/2} \cos\frac{\pi\,(p'-p)}{\Delta p}\,\frac{\hat{\Phi}_2 u_1(p')}{\exp\left(ik\bar{\Psi}'(p)\right)}\exp\left(-ik\xi p'\right)\,dp', \tag{3.8}$$

where $\Delta p = 1.0$ km. The spectral maxima is locate near $\xi = 0$. The tropospheric error of bending angle $\delta\epsilon_T(p)$ is estimated as the spectral width:

$$\delta\epsilon_T(p) = \left(\frac{\int |w(p,\xi)|^2\,\xi^2 d\xi}{\int |w(p,\xi)|^2\,d\xi}\right)^{1/2}. \tag{3.9}$$

Mean square error $\delta\epsilon(p)$ of the determination of bending angle was assumed to equal $\delta\epsilon_I(p)$ for ray heights $p - r_E > 10$ km, and $\delta\epsilon_T(p)$ for ray height $p - r_E < 10$ km.

Inversion and Estimation of Temperature Retrieval Errors

From the neutral bending angles $\epsilon(p)$, by the Abel inversion (2.4), the refractivity $n(r)$ is retrieved. The dispersion of the retrieved refractivity is estimated as follows:

$$\left\langle \delta n^2(x)\right\rangle = \int_x^\infty\!\!\int \frac{\langle \delta\epsilon(p')\delta\epsilon(p'')\rangle\;dp'dp''}{\sqrt{p'^2 - x^2}\sqrt{p''^2 - x^2}}, \tag{3.10}$$

where the covariance matrix of the bending angles $\langle \delta\epsilon(p')\delta\epsilon(p'')\rangle$ is assumed to equal $\delta\epsilon^2(p)$ if $p' = p'' = p$, and for other values of p' and p'', the covariance matrix was taken in the triangle shape with a characteristic width 1 km according to the estimation in [42].

For the errors of the retrieved temperature, from (2.6) we readily derive the following estimation:

$$\left\langle \delta T^2(z) \right\rangle = \frac{\left\langle \delta n^2(z) \right\rangle}{\left[n(z)-1\right]^2} T^2 - 2\frac{\int_z^\infty g(z')\ \left\langle \delta n(z)\delta n(z') \right\rangle\ dz'}{R\left[n(z)-1\right]^2} T + \\ + \frac{\iint_z^\infty g(z'')g(z')\ \left\langle \delta n(z')\delta n(z'') \right\rangle\ dz'\,dz''}{R^2\left[n(z)-1\right]^2}. \quad (3.11)$$

Assuming that the correlation radius of error $\delta n(z)$ is significantly smaller that the homogeneous atmosphere height, we can approximately write:

$$\left\langle \delta T^2 \right\rangle^{1/2} = \left\langle \delta n^2 \right\rangle^{1/2} \frac{T}{n-1}. \quad (3.12)$$

Analysis of Observational Data

In this Chapter we discuss examples of processing occultation events observed by CHAMP. We compute bending angles and temperature profiles and their error estimates from formulas (3.9) and (3.12). We also give the bending angles and temperature profiles computed from the global atmospheric fields from the analysis of German Weather Service (Deutscher WetterDienst – DWD) nearest in time. It is important to notice that the discrepancy between the radio occultation data and DWD data includes both errors of radio occultation data and error of the analysis. The comparison of radio occultation data with analyses of European Center for Middle-Range Weather Forecast based on the statistical analysis of a large number of occultation events was presented in [7, 38]. Here we do not perform such a statistical comparison.

Figure 3.1, panels c) and d), shows the bending angles and temperatures retrieved from a CHAMP occultation event, as well as the estimates of their errors. Above 25 km, the estimates of the error due to background ionospheric fluctuations begin to increase. Above 30–40 km radio occultation data do provide useful information for weather forecast [41, 42]. Between 25 km and 7 km the estimates of the errors are mostly limited by 1 K. This is explained by the fact that in this height range bending angles large enough as compared to the background ionospheric fluctuations, and multipath propagation effects for GPS frequencies do not play any noticeable role. Below 7 km, multipath propagation emerges, as indicated by the non-monotonous bending angle profiles retrieved from the CHAMP data, as well as modelled for the DWD analysis. Here, the estimations of the errors significantly increase.

Figure 3.2 shows the results of processing another occultation event. Here the profile of the bending angle is non-monotonous in the impact parameter intervals of 11–12 and 6–8 km. Here the estimate of the errors of the bending angle profile proves to be low enough to draw a conclusion about multipath propagation. In the L2 channel the deterioration of the data quality in this intervals is noticed. Below 4 km, in the area of strong multipath, the estimates of the bending angle errors are significant. In this event, the ionospheric fluctuations are weak, and the estimation of the temperature retrieval error at a height of 30 km is about 1 K.

4 Conclusion

In this Report we described the methods of interpretation of data of radio occultation sounding of the Earth's atmosphere. The methods include: 1) noise reduction and quality control of L2 data on the

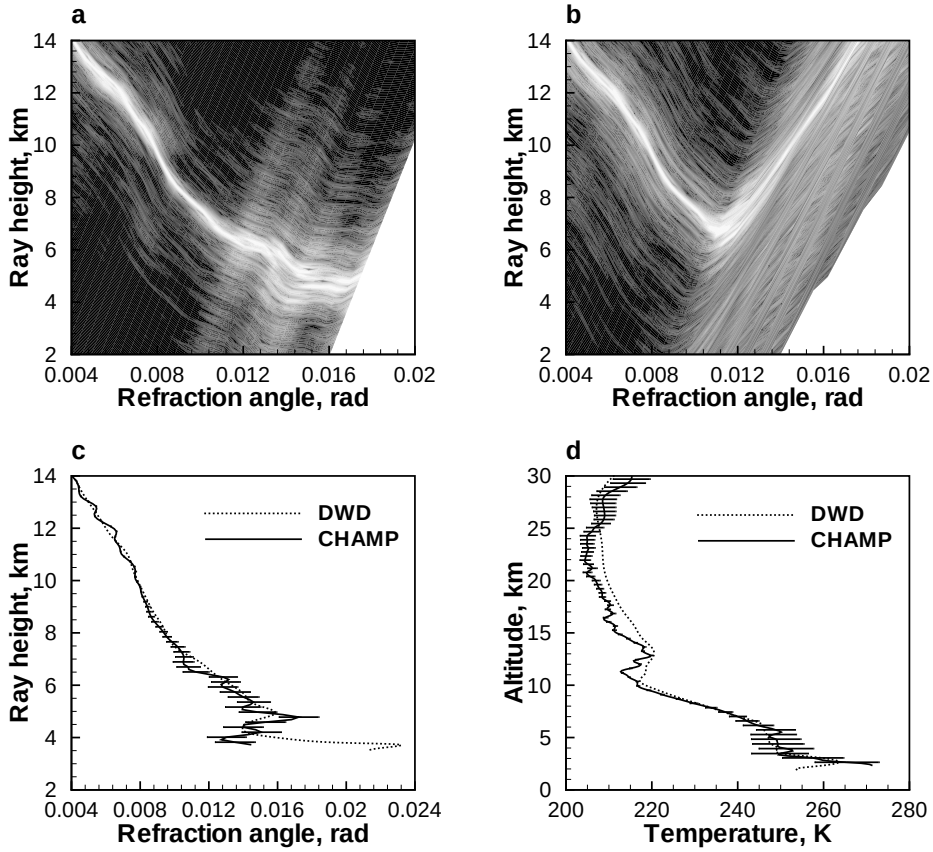

Figure 3.1: Radio occultation event 0004, January 18, 2004, UTC 00:24, 50.4°N 116.1°W: a) local spatial spectra for L1 channel, b) local spatial spectra for L2 channel, c) bending angles: computed for the DWD analysis and retreived from the CHAMP data, d) temperature from the DWD analysis and retrieved from the CHAMP data.

basis of the analysis of local spatial spectra of measured wave fields; 2) the retrieval of bending angles by the CT method; 3) the estimation of errors of bending angles by the analysis of the local spectra of the wave field in the transformed space; 4) ionospheric correction combined with the statistical regularization; 5) Abel inversion of bending angle profiles for the retrieval of refractivity, 6) retrieval of temperature profile in the hydrostatic approximation. It is important that the error estimations can be obtained without using a priori information. At big heights ionospheric fluctuations prevail in the signal. This allows for the estimation of bending angle errors above 8–10 km, where ionospheric fluctuation are the main error source. Below 8–10 km, errors of the derivation of bending angles are due to multipath propagation. These errors are estimated from the width of the local spatial spectra of the measured wave field. Errors due to multipath prove to be significant in the lower troposphere. This indicates that the receiver currently in use needs enhancement. However, this problem is not principle, it is technical, and upon the opinion of the majority of the specialists for radio occultations, it can be resolved by implementing open loop signal tracking. The final purpose of the development of the algorithms for data processing and error estimation is their application in a system of variational assimilation of radio occultation data into a model of global atmospheric circulation. The work on the implementation of the described algorithms in the data assimilation system of DWD is being performed currently.

Acknowledgement 1 *The Author is grateful to A. S. Gurvich, V. I. Klyatskin, I. G. Yakushkin, S. V. Sokolovskiy (Obukhov Institute for Atmospheric Physics, Russian Academy of Sciences), Yu. A. Kravtsov (Space Research Institute, Russian Academy of Sciences), A. S. Jensen and K. B. Lauritsen*

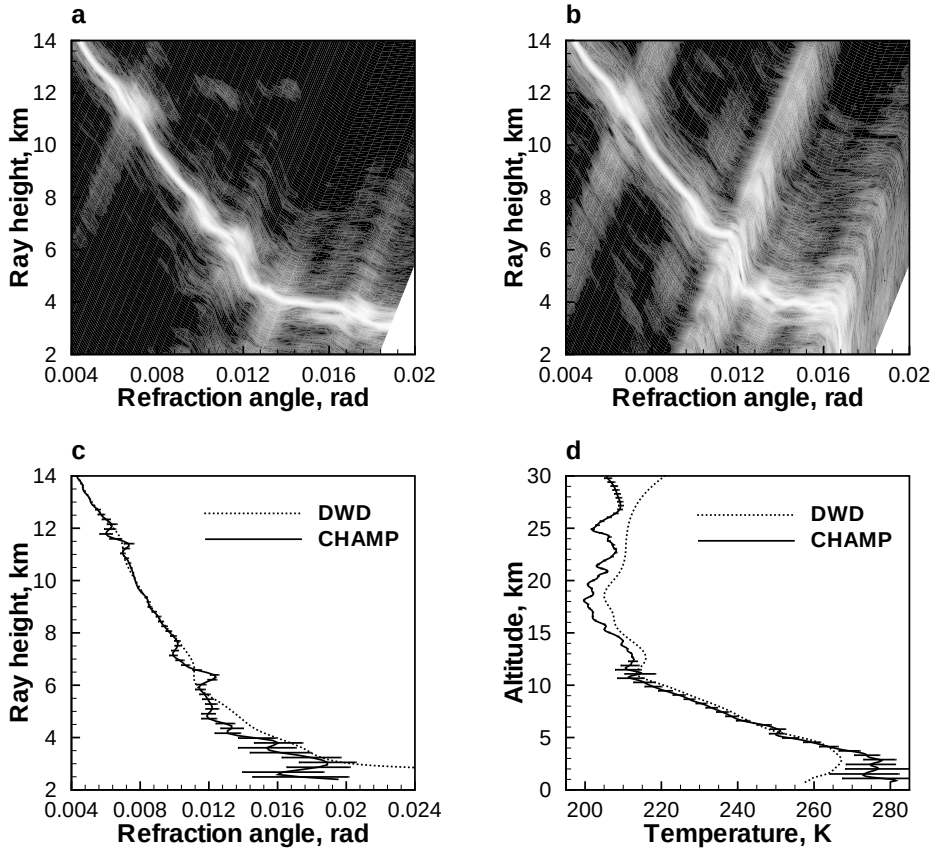

Figure 3.2: Radio occultation event 0008, January 18, 2004, UTC 00:48, 37.1°N 60.2°E: a) local spatial spectra for L1 channel, b) local spatial spectra for L2 channel, c) bending angles: computed for the DWD analysis and retreived from the CHAMP data, d) temperature from the DWD analysis and retrieved from the CHAMP data.

(Danish Meteorological Institute) for a valuable scientific discussion. The work was funded by German Weather Service and Danish Meteorological Institute.

Bibliography

[1] E. R. Kursinski, G. A. Hajj, S. S. Leroy, B. Herman. The GPS radio occultation technique. *Terrestr. Atmosph. Ocean. Sci.*, 11(1):53–114, 2000.

[2] A. S. Gurvich, T. G. Krasil'nikova. Navigation satellites for radio sensing of the Earth's atmosphere. *Soviet Journal of Remote Sensing*, 7(6):1124–1131, In Russian 1987, In English 1990.

[3] E. R. Kursinski, G. A. Hajj, W. I. Bertiger, S. S. Leroy, T. K. Meehan, L. J. Romans, J. T. Schofield, D. J. McCleese, W. G. Melbourne, C. L. Thornton, T. P. Yunck, J. R. Eyre, R. N. Nagatani. Initial results of radio occultation observation of Earth's atmosphere using the global positioning system. *Science*, 271:1107–1110, 1996.

[4] R. Ware, M. Exner, D. Feng, M. Gorbunov, K. Hardy, B. Herman, Y.-H. Kuo, T. Meehan, W. Melbourne, C. Rocken, W. Schreiner, S. Sokolovsky, F. Solheim, X. Zou, R. Anthes, S. Businger, K. Trenberth. GPS sounding of the atmosphere from Low Earth Orbit: Preliminary results. *Bulletin of the American Meteorological Society*, 77(1):19–40, 1996.

[5] C. Rocken, R. Anthes, M. Exner, D. Hunt, S. Sokolovsky, R. Ware, M. Gorbunov, W. Schreiner, D. Feng, B. Herman, Y.-H. Kuo, X. Zou. Analysis and validation of GPS/MET data in the neutral atmosphere. *Journal of Geophysical Research*, 102(D25):29849–29866, 1997.

[6] A. K. Steiner, G. Kirchengast, H. P. Ladreiter. Inversion, error analysis, and validation of GPS/MET data. *Ann. Geophys.*, 17:122–138, 1999.

[7] M. E. Gorbunov, L. Kornblueh. Analysis and validation of GPS/MET radio occultation data. *Journal of Geophysical Research*, 106(D15):17,161–17,169, 2001.

[8] J. Wickert, C. Reigber, G. Beyerle, R. Konig, C. Marquardt, T. Schmidt, L. Grunwaldt, R. Galas, T. K. Meehan, W. G. Melbourne, K. Hocke. Atmosphere sounding by GPS radio occultation: First results from CHAMP. *Geophys. Res. Lett.*, 28(17):3263–3266, 2001.

[9] J. R. Eyre. Assimilation of radio occultation measurements into a numerical weather prediction system. Technical Memorandum No. 199, European Center for Medium-Range Weather Forecast, 1994.

[10] X. Zou, Y.-H. Kuo, Y.-R. Guo. Assimilation of atmospheric radio refractivity using a nonhydrostatic adjoint model. *Monthly Weather Review*, 123:2229–2249, 1995.

[11] H. Liu, X. Zou. Improvements to a GPS radio occultation ray-tracing model and their impacts on assimilation of bending angle. *J. Geophys. Res.*, 108(D17):4548, doi: 10.1029/2002JD003160, 2003.

[12] M. E. Gorbunov, L. Kornblueh. Principles of variational assimilation of GNSS radio occultation data. Report No. 350, Max Planck Institute for Meteorology, Hamburg, December 2003.

[13] V. V. Vorob'ev, T. G. Krasil'nikova. Estimation of the accuracy of the atmospheric refractive index recovery from Doppler shift measurements at frequencies used in the NAVSTAR system. *Izvestiya Academy of Sciences SSSR, Atmospheric and Oceanic Physics, English Translation*, 29(5):602–609, 1994.

[14] A. G. Pavelyev. On the feasibility of radioholographic investigations of wave fields near the Earth's radio-shadow zone on the satellite-to-satellite path. *J. of Comm. Techn. and Elec.*, 43(8):875–879, 1998.

[15] K. Igarashi, A. Pavelyev, K. Hocke, D. Pavelyev, I. A. Kucherjavenkov, S. Matyugov, A. Zakharov, O. Yakovlev. Radio holographic principle for observing natural processes in the atmosphere and retrieving meteorological parameters from radio occultation data. *Earth, Planets, and Space*, 52(11):893–899, 2000.

[16] A. G. Pavelyev, Y. A. Liou, J. Wickert. Diffractive vector and scalar integrals for bistatic radio holographic remote sensing. *Radio Science*, 39(4):RS4011, doi:10.1029/2003RS002935, 2004.

[17] M. E. Gorbunov. Canonical transform method for processing GPS radio occultation data in lower troposphere. *Radio Sci.*, 37(5):9–1–9–10, doi:10.1029/2000RS002592, 2002.

[18] A. S. Jensen, M. S. Lohmann, H.-H. Benzon, A. S. Nielsen. Full spectrum inversion of radio occultation signals. *Radio Sci.*, 38(3):6–1–6–15, doi: 10.1029/2002RS002763, 2003.

[19] M. E. Gorbunov, K. B. Lauritsen. Canonical transform methods for radio occultation data. Scientific Report 02-10, Danish Meteorological Institute, Copenhagen, Denmark, 2002. http://www.dmi.dk/dmi/Sr02-10.pdf.

[20] A. S. Jensen, M. S. Lohmann, A. S. Nielsen, H.-H. Benzon. Geometrical optics phase matching of radio occultation signals. *Radio Sci.*, 39(3):RS3009, doi: 10.1029/2003RS002899, 2004.

[21] S. V. Sokolovskiy. Modeling and inverting radio occultation signals in the moist troposphere. *Radio Sci.*, 36(3):441–458, 2001.

[22] S. V. Sokolovskiy. Tracking tropospheric radio occultation signals from low earth orbit. *Radio Sci.*, 36(3):483–498, 2001.

[23] G. Beyerle, M. E. Gorbunov, C. O. Ao. Simulation studies of GPS radio occultation measurements. *Radio Sci.*, 38(5):1084, doi: 10.1029/2002RS002800, 2003.

[24] M. E. Gorbunov, S. V. Sokolovskiy. Remote sensing of refractivity from space for global observations of atmospheric parameters. Raport instytutowy Report No. 119, Max-Planck Institute for Meteorology, Hamburg, 1993.

[25] M. E. Gorbunov, A. S. Gurvich. Remote sending of the atmosphere using a system of synchronously orbiting satellites. *Radio Science*, 28(4):595–602, 1993.

[26] R. A. Phinney, D. L. Anderson. On the radio occultation method for studying planetary atmospheres. *Journal of Geophysical Research*, 73(5):1819–1827, 1968.

[27] B. R. Bean, E. J. Datton. *Radio meteorology*. Dover Publ. Inc., New-York, 1968.

[28] G. F. Lindal, J. R. Lyons, D. N. Sweetnam, V. R. Eshleman, D. P. Hinson, G. L. Tyler. The atmosphere of Uranus: Results of radio occultation measurements with Voyager. *Journal of Geophysical Research*, 92(A13):14987–15001, 1987.

[29] M. E. Gorbunov, A. S. Gurvich, L. Kornblueh. Comparative analysis of radioholographic methods of processing radio occultation data. *Radio Science*, 35(4):1025–1034, 2000.

[30] M. E. Gorbunov. Radioholographic analysis of radio occultation data in multipath zones. *Radio Sci.*, 37(1):14–1–14–9, doi: 10.1029/2000RS002577, 2002.

[31] M. E. Gorbunov. Radio-holographic analysis of Microlab-1 radio occultation data in the lower troposphere. *J. Geophys. Res. - Atm.*, 107(D12):7–1–7–10, doi: 10.1029/2001JD000889, 2002.

[32] Yu. A. Kravtsov, Yu. I. Orlov. *Geometrical optics of inhomogeneous media*. Springer, Berlin, 1990.

[33] A. S. Mishchenko, V. E. Shatalov, B. Yu. Sternin. *Lagrangian manifolds and the Maslov operator*. Springer-Verlag, Berlin - New York, 1990.

[34] V. I. Arnold. *Mathematical Methods of Classical Mechanics*. Springer-Verlag, New York, 1978.

[35] M. E. Gorbunov, K. B. Lauritsen. Analysis of wave fields by Fourier Integral Operators and its application for radio occultations. *Radio Sci.*, 39(4):RS4010, doi:10.1029/2003RS002971, 2004. accepted.

[36] V. R. Eshleman, D. O. Muhleman, P. D. Nicholson, P. G. Steffes. Comment on absorbing regions in the atmosphere of Venus as measured by radio occultation. *Icarus*, 44:793–803, 1980.

[37] C. O. Ao, T. K. Meehan, G. A. Hajj, A. J. Mannucci, G. Beyerle. Lower-troposphere refractivity bias in GPS occultation retrievals. *J. Geophys. Res.*, 108(D18):4577, doi:10.1029/2002JD003216, 2003.

[38] M. E. Gorbunov, L. Kornblueh. Analysis and validation of Challenging Minisatellite Payload (CHAMP) radio occultation data. *J. Geophys. Res.*, 108(D18):4584, doi:10.1029/2002JD003175, 2003.

[39] S. Sokolovskiy, D. Hunt. Statistical optimization approach for GPS/MET data inversions. *URSI GPS/MET Workshop*, Tucson, AZ, 1996.

[40] S. Syndergaard. On the ionospheric calibration in GPS radio occultation measurements. *Radio Sci.*, 35(3):865–883, 2000.

[41] M. E. Gorbunov. Ionospheric correction and statistical optimization of radio occultation data. *Radio Sci.*, 37:17–1–17–9, doi: 10.1029/2000RS002370, 2002.

[42] V. V. Vorob'ev, V. Kan. Background fluctuations measured by the radio sounding of the ionosphere in the GPS-Microlab-1 experiment. *Izvestiya Visshykh Uchebnykh Zavedeniy, Radiofizika*, XLII(6):511–523, 1999.

[43] I. N. Bronstein, K. A. Semendjajew. *Taschenbuch der Mathematik*. B. G. Teubner Verlaggesellschaft, Leipzig, 1983.

[44] Yu. V. Egorov. *Lectures on Partial Differential Equations. Additional Chapters*. Moscow State University Press, Moscow, 1985. (In Russian).

[45] V. I. Tatarskii. *Wave propagation in a turbulent medium*. MacGraw-Hill, New York, 1961.

[46] V. F. Turchin, V. Z. Nozik. Statistical regularization of the solution of incorrectly posed problems. *Izvestiya Academy of Sciences SSSR, Atmospheric and Oceanic Physics, English Translation*, 5(1):14–18, 1969.